Theoretical Calculations of the Electronic Absorption Spectra of Oxotitanium(IV) Phthalocyanine in the Solid State

Katsunori Nakai, Kazuyuki Ishii, and Nagao Kobayashi*

Department of Chemistry, Graduate School of Science, Tohoku University, Sendai 980-8578, Japan

Hisatomo Yonehara and Chyongjin Pac

Kawamura Institute of Chemical Research, 631 Sakado, Sakura, Chiba 285-0078, Japan

Received: June 2, 2003; In Final Form: July 10, 2003

Oxotitanium(IV) phthalocyanine (OTiPc) has been reported to be a near-IR-active photoconductor, where crystal modifications termed phases I, II, and Y exist. In this paper, solid-state electronic absorption spectra of OTiPc have been theoretically calculated by considering three origins (i.e., exciton, charge transfer (CT), and molecular distortion) to clarify the crystal form dependence on the large red shift of the Q absorption band and high photoconductivity of the photoactive phase II in particular. In these calculations, intermolecular interactions are included in the form of configuration interactions between exciton and CT configurations, and matrix elements were calculated using the ZINDO/S Hamiltonian in order to calculate 3D metallocomplexes. By considering 243 neighboring OTiPc molecules, our theoretical calculations have succeeded in reproducing the experimental trends of the solid-state optical properties, such as the large red shift of the Q absorption band, dependence on the incident light direction, phase dependence, and CT character, indicating the reliability of our calculations. In addition, it is demonstrated that the photoconductive properties correlate well with intermolecular resonance integrals. Calculations shown here are useful not only for understanding the solid-state electronic structures of OTiPc but also for designing new functional molecular crystals.

Introduction

Since their first synthesis almost a century ago, phthalocyanine (Pc) derivatives have attracted attention as a result of their diverse electronic, optical, and structural properties, which offer applications in the fields of nonlinear optics,[1] catalysis,[2] liquid crystals,[3] electrochromism,[4] sensors,[5] photosensitizers,[6] molecular electronics,[7] photovoltaic cells,[8] Langmuir−Blodgett films,[9] semiconductors, [10] and photoconductor devices.[11] In some of these modern applications such as photovoltaic cells and photoconductor devices, the crystal structure can have a significant influence on their efficiency.[8,12,13] Indeed, solid-state electronic absorption spectra of Pc thin films have been known to produce the broadened and red-shifted Q band depending on the crystal structure.[11−15] For instance, in the case of oxotitanium(IV) phthalocyanine (OTiPc) being used in GaAsAl laser printers as a near-IR photoconductor,[12−14,17−19] of the three crystal modifications termed phases I, II, and Y (phases I and II correspond to phases β and α, respectively) phases II and Y are photoactive in the near-IR region. Although the crystal structure of phase Y is still unclear, crystal structures of phases I and II and their thin film solid-state electronic absorption spectra have been clarified, as shown in Figure 1.[14,18] A broad electronic absorption band seen at around 770 nm for photoinactive phase I shifts to 850 nm in photoactive phase II. Since the correlation between the large red shift and high photoconductivity in phase II evoked a great deal of interest, the relationship between crystal structures, photoconductivity, and optical properties of Pcs has been intensively investigated. Armstrong and co-workers have investigated the electronic absorption spectra of epitaxially deposited MPcCl thin films (M = Al, Ga, and In).[15] They calculated the spectral peaks of the ordered multilayer Pc thin films by the summation of the transition dipole interactions, which was extended into three dimensions. Saito et al. have measured electroabsorption spectra of MPc (M = OTi and Cu) thin films to distinguish Frenkel exciton from charge transfer (CT) transitions.[12a] In photoactive phases II and Y of OTiPc, electroabsorption signals attributable to CT bands were seen at around 830 nm, which correlated well with the free-carrier generation efficiency. However, Mizuguchi et al. have investigated solid-state absorption spectra of OTiPc on the basis of configuration interaction (CI) calculations of a single molecule.[19] They suggested that differences in optical spectra between phases I and II can be interpreted mainly in terms of molecular distortion. As stated above, although intermolecular interactions, exciton and CT, and molecular distortion have previously been listed, the origins of the crystal form dependence of, for example, the large red shift of the Q absorption band and high photoconductivity of phase II are still unclear and therefore in need of elucidation.

In this paper, we have theoretically calculated the solid-state electronic absorption spectra of OTiPc by considering these three origins (i.e., exciton, CT, and molecular distortion). Although the Davydov splitting is well known in the theory of molecular crystals,[20] it is not sufficient to take into account the CT character in the solid state of OTiPc. Parson and Warshel et al. calculated the absorption spectra of methylbacteriopheophorbide

* Corresponding author. E-mail: nagaok@mail.tains.tohoku.ac.jp.

10.1021/jp035533j CCC: $25.00
Published on Web 08/13/2003

a crystals using the QCFF/PI method,[21] where π molecular orbitals of individual molecules are written as linear combinations of atomic orbitals and intermolecular interactions are included in the form of configuration interactions between exciton and CT configurations. With reference to their approach, we have employed both exciton and CT configurations and have calculated matrix elements using the ZINDO/S Hamiltonian, which can be used to calculate 3D metallocomplexes.[22] Thus, molecular distortion, exciton, and CT interactions in solid-state OTiPc are investigated not only for reproducing optical spectra but also from the viewpoint of photoconductivity.

Calculation Methods

i. Molecular Orbitals and Basis Functions. Molecular orbitals of individual OTiPc molecules written as linear combinations of atomic orbitals were calculated using the ZINDO/S Hamiltonian (HyperChem program package).[23] Here, molecular structures determined by X-ray crystallographic analyses (Chart 1) were used for phases I and II.[18] Positions of hydrogens were determined using the "add hydrogen" program in the HyperChem program package.[23]

As basis functions in molecular crystal, we employed both exciton and CT configurations.[21] In the case of exciton configurations, the two lowest excited singlet states, Q_1 and Q_2 ($\psi_{Q1}{}^a$, $\psi_{Q2}{}^a$), were considered for individual isolated OTiPc *a* because only these excitation energies occur in the visible region. The Q_1 and Q_2 states consist mainly of $HOMO^a \rightarrow LUMO^a$ and $HOMO^a \rightarrow LUMO+1^a$ configurations, respectively.[24]

In the case of CT configurations, four CT configurations between OTiPc *a* and the neighboring *b* were considered, i.e., $HOMO^a \rightarrow LUMO^b$($\psi_{CT1}{}^{ab}$), $HOMO^a \rightarrow LUMO + 1^b$($\psi_{CT2}{}^{ab}$), $HOMO^b \rightarrow LUMO^a$($\psi_{CT1}{}^{ba}$), and $HOMO^b \rightarrow LUMO + 1^a$-($\psi_{CT2}{}^{ba}$). When molecules were further apart, the CT configurations were neglected. In addition, upper CT configurations such as $HOMO - 1^a \rightarrow LUMO^b$ were also neglected because of the high energy.

ii. Matrix Elements. By considering the exciton and CT configurations, we can write the configuration interactions as a matrix *U* as follows.

At the start, diagonal energies are illustrated. The $E_{Q1}{}^i$ and $E_{Q2}{}^i$ energies of molecule *i* were evaluated in terms of the CI calculations of individual OTiPc molecules using the ZINDO/S Hamiltonian (Reimers' program).[25] In these calculations, 400 configurations including singly and doubly excited configurations were considered. The CT energies between molecules *i* and *j*, $E_{CT1}{}^{ij}$ and $E_{CT2}{}^{ij}$, are represented as follows.

$$E_{CT1}{}^{ij} = E_{LUMO}{}^{j} - E_{HOMO}{}^{i} - \langle \phi_{HOMO}{}^{i} \phi_{LUMO}{}^{j} \mid \phi_{HOMO}{}^{i} \phi_{LUMO}{}^{j} \rangle \quad (2a)$$

$$E_{CT2}{}^{ij} = E_{LUMO+1}{}^{j} - E_{HOMO}{}^{i} - \langle \phi_{HOMO}{}^{i} \phi_{LUMO+1}{}^{j} \mid \phi_{HOMO}{}^{i} \phi_{LUMO+1}{}^{j} \rangle \quad (2b)$$

$$\langle \phi_m \phi_n \mid \phi_p \phi_q \rangle = \int\int \phi_m(1)\, \phi_n(2) \left(\frac{e^2}{r_{12}}\right) \phi_p(1)\, \phi_q(2)\, d\tau_1\, d\tau_2 \quad (2c)$$

Here, $E_m{}^i$ and $\phi_m{}^i$ denote the energy and wave function for molecular orbital *m* of molecule *i*, respectively, which were calculated using the ZINDO/S method (HyperChem program package).[23] The last term corresponding to the intermolecular Coulomb integral was calculated under the ZINDO/S approximation.[22] Because the electric transition dipole moment is zero in the case of a pure CT configuration,[12,21] the absorption intensity of CT bands originates from an admixture between the exciton and CT configurations.

Off-diagonal matrix elements are divided into three parts: U^{LOC}, U^{LOC-CT}, and U^{CT}. U^{LOC} reflects intermolecular exciton interactions. The exciton interaction between molecules *i* and *j* is represented under a point-dipole approximation as follows.[15]

$$\langle \psi_{Qk}{}^{i} | H | \psi_{Ql}{}^{j} \rangle = \frac{(\mu_{Qk}{}^{i} \cdot \mu_{Ql}{}^{j})}{|\mathbf{r}_{ij}|^3} - \frac{3(\mu_{Qk}{}^{i} \cdot \mathbf{r}_{ij})(\mu_{Ql}{}^{j} \cdot \mathbf{r}_{ij})}{|\mathbf{r}_{ij}|^5} \quad (3)$$

Here, $\mu_{Qk}{}^i$ denotes the transition dipole moment of the Q_k band of molecule *i*. $\mathbf{r}_{ij}$ reflects the position vector between molecules *i* and *j*, which approximates to the position vector between Ti atoms of molecules *i* and *j*.

$$U = \begin{array}{c} \begin{array}{cccccccccc} \psi_{Q1}{}^a & \psi_{Q2}{}^a & \psi_{Q1}{}^b & \psi_{Q2}{}^b & \cdots\cdots & \psi_{CT1}{}^{ab} & \psi_{CT2}{}^{ab} & \psi_{CT1}{}^{ba} & \psi_{CT2}{}^{ba} & \cdots\cdots \end{array} \\ \begin{bmatrix} E_{Q1}{}^a & U^{LOC} & & U^{LOC-CT} \\ & E_{Q2}{}^a & & \\ U^{LOC} & E_{Q1}{}^a & & \\ & U^{LOC} & E_{Q2}{}^a & \\ U^{CT-LOC} & & E_{CT1}{}^{ab} & U^{CT} \\ & & E_{CT2}{}^{ab} & \\ & & U^{CT} & E_{CT1}{}^{ba} \\ & & & U^{CT} \quad E_{CT2}{}^{ba} \end{bmatrix} \end{array} \quad (1)$$

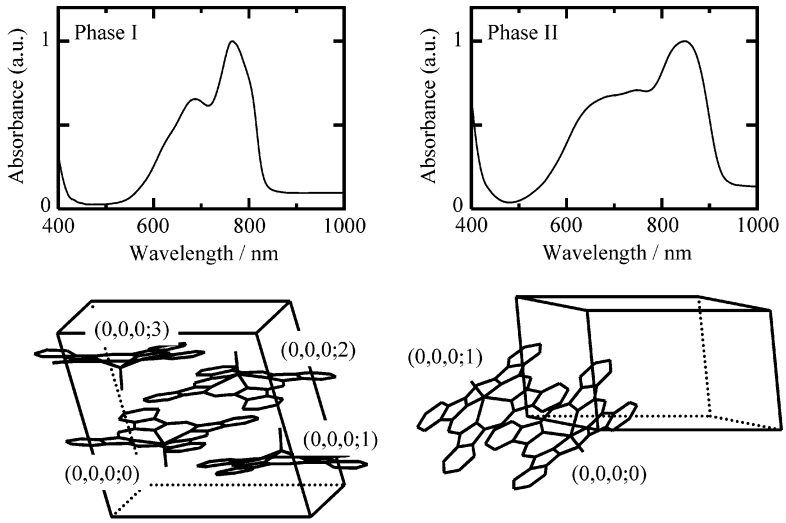

Figure 1. Visible−near-infrared transmission−absorption spectra of OTiPc for the incident light direction being perpendicular to the crystallographic *ac* plane of phase I (top left) and the *ac* plane of phase II (top right) with molecular structures in the unit cell of phase I (bottom left) and phase II (bottom right).[14,18]

CHART 1

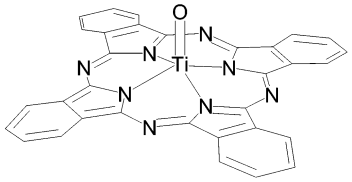

Off-diagonal matrix elements between the exciton and CT configurations, $U^{\mathrm{LOC-CT}}$, correspond to intermolecular resonance integrals.[21] Because it is known that the Q bands of OTiPc consist almost entirely of HOMO → LUMO or HOMO → LUMO + 1 configurations (>90% in our CIS calculations), $U^{\mathrm{LOC-CT}}$ reasonably approximated to a single resonance integral, β, as follows.

$$\langle \psi_{\mathrm{Q}k}{}^{g}|H|\psi_{\mathrm{CT}l}{}^{ij}\rangle =$$

$$\begin{aligned}
&\langle \phi_{\mathrm{LUMO}}{}^{i}|H_{\mathrm{core}}|\phi_{\mathrm{LUMO}}{}^{j}\rangle = \beta_{\mathrm{LL}}{}^{ij} && (g=i,\ k=l=1)\\
&\langle \phi_{\mathrm{LUMO+1}}{}^{i}|H_{\mathrm{core}}|\phi_{\mathrm{LUMO+1}}{}^{j}\rangle = \beta_{\mathrm{L+1L+1}}{}^{ij} && (g=i,\ k=l=2)\\
&-\langle \phi_{\mathrm{HOMO}}{}^{i}|H_{\mathrm{core}}|\phi_{\mathrm{HOMO}}{}^{j}\rangle = -\beta_{\mathrm{HH}}{}^{ij} && (g=j,\ k=\mathrm{l})\\
&\langle \phi_{\mathrm{LUMO}}{}^{i}|H_{\mathrm{core}}|\phi_{\mathrm{LUMO+1}}{}^{j}\rangle = \beta_{\mathrm{LL+1}}{}^{ij} && (g=i,\ k=1,\ l=2)\\
&\langle \phi_{\mathrm{LUMO+1}}{}^{i}|H_{\mathrm{core}}|\phi_{\mathrm{LUMO}}{}^{j}\rangle = \beta_{\mathrm{L+1L}}{}^{ij} && (g=i,\ k=2,\ l=1)\\
&0 && (g=j,\ k\neq l \text{ or } g\neq i,\ g\neq j)
\end{aligned} \tag{4}$$

Here, H_{core} corresponds to the core Hamiltonian. The magnitude of β values rapidly decreases with increasing intermolecular distance.[21] In addition, only CT configurations that can admix with dipole-allowed exciton configurations are needed to reproduce the electronic absorption spectra. For these reasons, only CT configurations between neighboring OTiPc molecules are considered.

In the case of CT−CT interaction, the off-diagonal matrix elements, U^{CT}, are represented as follows.

$$\langle \psi_{\mathrm{CT}k}{}^{fg}|H|\psi_{\mathrm{CT}l}{}^{ij}\rangle =$$

$$\begin{aligned}
&\langle \phi_{\mathrm{LUMO}}{}^{g}|H_{\mathrm{core}}|\phi_{\mathrm{LUMO}}{}^{j}\rangle = \beta_{\mathrm{LL}}{}^{gj} && (f=i,\ g\neq j,\ k=l=1)\\
&\langle \phi_{\mathrm{LUMO+1}}{}^{g}|H_{\mathrm{core}}|\phi_{\mathrm{LUMO+1}}{}^{j}\rangle = \beta_{\mathrm{L+1L+1}}{}^{gj} && (f=i,\ g\neq j,\ k=l=2)\\
&-\langle \phi_{\mathrm{HOMO}}{}^{f}|H_{\mathrm{core}}|\phi_{\mathrm{HOMO}}{}^{i}\rangle = -\beta_{\mathrm{HH}}{}^{fi} && (f\neq i,\ g=j,\ k=l)\\
&\langle \phi_{\mathrm{LUMO}}{}^{g}|H_{\mathrm{core}}|\phi_{\mathrm{LUMO+1}}{}^{j}\rangle = \beta_{\mathrm{LL+1}}{}^{gj} && (f=i,\ g\neq j,\ k=1,\ l=2)\\
&\langle \phi_{\mathrm{LUMO+1}}{}^{g}|H_{\mathrm{core}}|\phi_{\mathrm{LUMO}}{}^{j}\rangle = \beta_{\mathrm{L+1L}}{}^{gj} && (f=i,\ g\neq j,\ k=2,\ l=1)\\
&\langle \phi_{\mathrm{HOMO}}{}^{i}\,\phi_{\mathrm{LUMO}}{}^{j}|\phi_{\mathrm{HOMO}}{}^{i}\,\phi_{\mathrm{LUMO+1}}{}^{j}\rangle && (f=i,\ g=j,\ k\neq \mathrm{l})\\
&0 && (f\neq i,\ g=j,\ k\neq \mathrm{l} \text{ or } f\neq i,\ g\neq j)
\end{aligned} \tag{5}$$

These matrix elements, β and Coulomb integrals, were also evaluated using the ZINDO/S Hamiltonian.[22] Using these matrix elements, the matrix U was diagonalized, and excited-state energies and oscillator strengths were calculated.

As a result, the line-shape function, $\epsilon(\nu)$, was expressed as follows.

$$\epsilon(\nu) = \sum_j F_j \cdot g(\nu - \nu_j) \tag{6a}$$

$$g(\nu - \nu_j) = (\sqrt{2\pi}\cdot s(\nu))^{-1} \exp\left[-\frac{(\nu-\nu_j)^2}{2\sigma(\nu)^2}\right] \tag{6b}$$

Here, F_j and ν_j denote the oscillator strength and transition energy of the jth transition, respectively. $g(\nu - \nu_j)$ is the Gaussian line-shape function for a single transition, where the bandwidth, $\sigma(\nu)$, was evaluated experimentally.[26]

Results and Discussion

i. Excited-State Energies of Individual OTiPc Molecules. Excited-state energies of individual OTiPc molecules have been

TABLE 1: Q-Band Energies Calculated Using the ZINDO/S Hamiltonian

	Q_1/nm (f^a)	Q_2/nm (f^a)
phase I (C_1)	685 (0.49)	694 (0.49)
phase II (C_1)	658 (0.39)	705 (0.45)
optimized geometry (C_{4v})	693 (0.52)	693 (0.52)
solution (obsd)[b]	690	

[a] f = oscillator strength. [b] From ref 27.

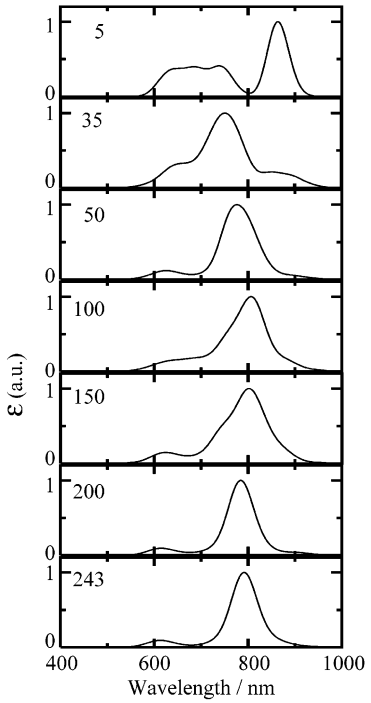

Figure 2. Calculated absorption spectra for the incident light direction being perpendicular to the crystallographic *ac* plane of phase II, where exciton interactions were calculated for $N = 5$, 35, 50, 100, 150, 200, and 243 neighboring OTiPc molecules.

calculated by considering 400 configurations, including singly and doubly excited configurations, as summarized in Table 1.[25,27] In the case of the OTiPc structure optimized using the PM3 Hamiltonian, the degenerate Q bands were calculated at 693 nm, which is almost identical to that (690 nm) observed in CH_2Cl_2 solution.[27] This indicates that our CI calculations can give a good reproduction of the Q-band energies of individual OTiPc molecules. However, experimental trends of solid-state absorption spectra, such as a broad bandwidth and large red shift, cannot be reproduced using only the CI calculations of individual OTiPc molecules, even when structures determined by X-ray analyses were used for phases I and II.[18] This does not agree with a previous investigation by Mizuguchi et al., where the large red shift in phase II could be interpreted mainly by the molecular distortion.[19] In their calculations, the Q bands were evaluated as 679 and 775 nm for an individual OTiPc molecule in phase II; these values are obviously different from our present calculations (658 and 705 nm). We interpreted this as being due to a difference between the singly and doubly excited configurations. The Q-band energies calculated using only singly excited configurations strongly depend on the number of configurations and shift to lower energy with an increasing number of configurations. That is, only the lowest excited-state energies stabilize, whereas the ground-state energy, which stabilizes as a result of interactions with the doubly excited configurations, is fixed. Therefore, the calculated Q-band energies lose credibility if the doubly excited configurations are not included. In contrast, when these are taken into consideration, the calculated Q-band energies are almost independent of the number of configurations and therefore are more reliable. In conclusion, the broad bandwidth and red shift in phase II cannot be interpreted using only molecular distortion, and the Q-band energies of individual OTiPc molecules are determined to be 685 and 694 nm for phase I and 658 and 705 nm for phase II.

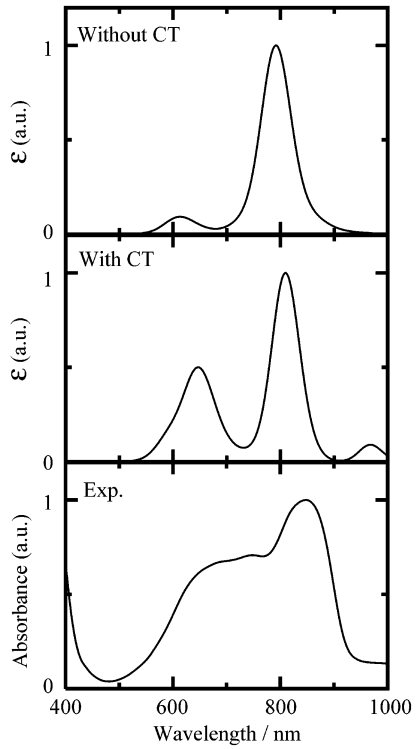

Figure 3. Calculated (top and middle) and observed (bottom) absorption spectra for the incident light direction being perpendicular to the crystallographic *ac* plane of phase II, where only exciton (top) or both exciton and CT (middle) configurations were taken into account.

ii. Intermolecular Interactions. To analyze exciton interactions in phase II, we have calculated all OTiPc molecules within a sphere of a given radius R around the central OTiPc. Here, the total number of neighboring molecules (N) was varied from 5 to 243. Calculated spectra are shown in Figure 2. Although the calculated spectra depend significantly on the number of molecules when the number is below 50, the spectral changes are relatively small when more than 100 molecules are considered (i.e., $R > 25$ Å). This is consistent with the previous calculation on methylbacteriopheophorbide *a* crystals.[21a] Therefore, all results presented below are based on calculations with $R = 33$ Å ($N = 243$ molecules). The calculated spectrum (including 243 molecules) shows a marked red shift (790 nm) compared with the calculated Q bands (658 and 705 nm) for individual OTiPc molecules, roughly reproducing the red-shifted position (850 nm, Figure 1) of the experimental Q-band peak. This suggests that the large red shift in phase II originates mainly from exciton interaction between neighboring OTiPc molecules. Thus, the CI calculations were carried out for phase II taking the CT configurations into consideration (Figure 3). In the calculated spectra with CT configurations, two intense bands are seen at around 810 and 650 nm, which are close to a peak (850 nm) and shoulder (650 nm), respectively, of the observed spectrum (Figure 3). Although the observed absorption band exhibits a continuous and broad band, in contrast to the calculated bands, this appears to originate from vibronic bands.

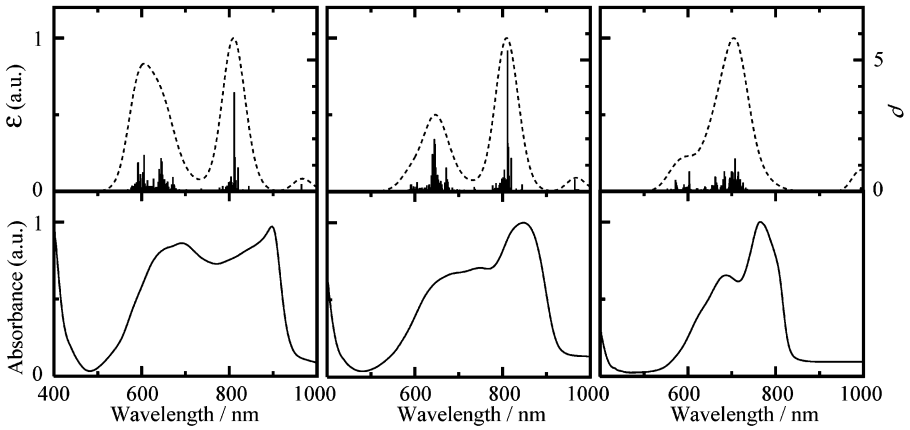

Figure 4. Calculated absorption spectra (- - -) for the incident light direction being perpendicular to the crystallographic *ab* plane of phase II (top left), *ac* plane of phase II (top center), and *ac* plane of phase I (top right) with experimental absorption spectra of OTiPc for the incident light direction being perpendicular to the crystallographic *ab* plane of phase II (bottom left), *ac* plane of phase II (bottom center), and *ac* plane of phase I (bottom right). Solid bars in the calculated spectra (top) denote the product of oscillator strengths and coefficients of CT configurations, ρ, as described in the text.

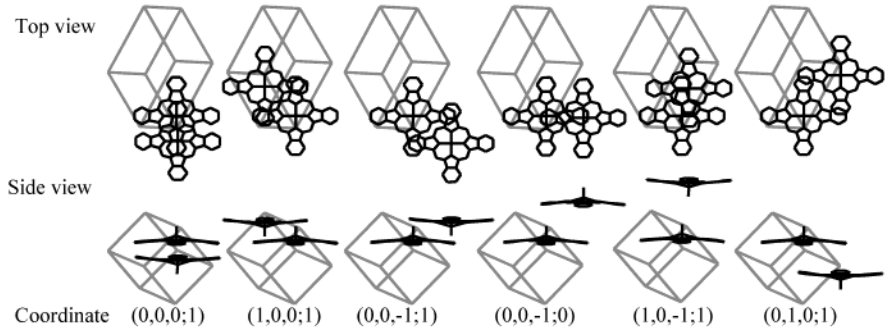

Coordinate	(0,0,0;1)	(1,0,0;1)	(0,0,-1;1)	(0,0,-1;0)	(1,0,-1;1)	(0,1,0;1)
$R_{Ti\text{-}Ti}$ (Å)	6.41	6.99	7.68	8.64	9.23	11.50
β_{HH} (cm^{-1})	398.5	1420.5	388.3	-0.3	0.0	-4.4
β_{LL}	409.8	431.8	422.2	5.6	-0.0	-0.2
β_{LL+1}	89.0	-760.5	-149.8	1.4	0.0	-4.1
β_{L+1L}	88.8	-761.3	-149.6	-0.7	0.0	-4.1
β_{L+1L+1}	-179.9	174.0	-434.1	4.0	-0.0	6.5

Figure 5. Summary of calculated resonance integrals with OTiPc at (0, 0, 0; 0) in phase II.

To confirm the reliability of our calculations, we calculated the dependence on the incident light direction, absorption spectrum of phase I, and contribution of CT character. In the case of phase II, absorption spectra were calculated for the incident light direction being perpendicular to the crystallographic *ab* and *ac* planes (Figure 4). In the observed absorption spectra, the absorbance ratio between 610 and 850 nm (= Abs(610)/Abs(850)) is larger for the incident light direction being perpendicular to the *ab* plane (bottom left) than for the direction being perpendicular to the *ac* plane (bottom center). This experimental trend is sufficiently reproduced by calculations where the band intensity at 610 nm is very close to that at 810 nm in the spectrum calculated for the incident light perpendicular to the *ab* plane (top left), and the intensity at 650 nm is one-half that at 810 nm in the spectrum calculated for the incident light perpendicular to the *ac* plane (top center).

To investigate the phase dependence, an absorption spectrum of phase I was also calculated and compared with that of phase II (Figure 4, top right, broken line). In our calculations, the intense band (810 nm) of phase II is lower in energy than that (710 nm) of phase I, reproducing the experimental large red shift of the Q band in phase II (770 and 850 nm for phases I and II, respectively). In addition, clear band splitting is not seen in the calculated spectrum of phase I in contrast to that in phase II, again consistent with the experimental observation that the absorption spectrum of phase II is broader than that of phase I. Although the peak positions of the calculated absorption spectra are higher in energy than those that are observed, our calculations reproduce the experimental trend of the phase dependence.

On the basis of the electroabsorption spectra of OTiPc thin films, Saito et al. suggested that electroabsorption signals attributable to CT bands appear at around 830 nm in phase II, in contrast to those in phase I.[12] To obtain information on the CT character, the products of oscillator strength and coefficients of CT configurations, ρ, were calculated for phases I and II, respectively. Calculated spectra are displayed using bars in Figure 4 (top). In the case of phase II, a large ρ value is seen at around 810 nm (top left and center), which is in good agreement with the electroabsorption results. However, in phase I (top, right), the calculated CT character is obviously smaller than that in phase II, which is also in accord with the electroabsorption results. A consideration of all of the data—these reproductions of the dependence on the incident light direction, phase dependence, and electroabsorption spectra—indicate that our calculations are reliable.

iii. Resonance Integrals. It is known that the CT character in the excited state dominates the photocarrier generation efficiency.[12,13] This does not contradict the fact that the CT band

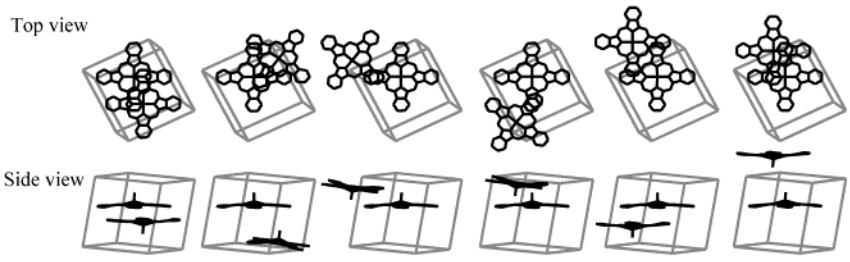

Coordinate	(0,0,0;2)	(0,0,0;3)	(-1,0,0;1)	(0,0,0;1)	(-1,0,0;2)	(-1,0,-1;2)
$R_{Ti\text{-}Ti}$ (Å)	7.20	9.29	9.53	9.59	9.73	9.76
β_{HH} (cm^{-1})	-1139.1	-0.1	335.3	79.0	-250.7	0.0
β_{LL}	54.5	-0.2	-329.4	-179.7	99.2	-0.0
β_{LL+1}	226.1	-0.1	189.5	56.8	48.0	0.0
β_{L+1L}	226.7	0.1	-16.2	76.5	48.1	0.0
β_{L+1L+1}	-719.9	-0.2	278.3	194.8	-184.4	-0.0

Figure 6. Summary of calculated resonance integrals with OTiPc at (0, 0, 0; 0) in phase I.

consists of the exciton and CT configurations, which correspond to photoexcitation and initial charge-separation processes, respectively. Because the admixture between the exciton and CT configurations is promoted by intermolecular resonance integrals, the β values are one of the most important parameters for photocarrier generation processes. Resonance integrals between OTiPc molecules are summarized in Figures 5 and 6, where crystallographic coordinates are shown by (r_a, r_b, r_c; x). The r_i's are integers, and a, b, and c form the edges of the crystal's unit cell. x is the molecular position in the unit cell. The resonance integral between OTiPc at (0, 0, 0; 0) and the neighboring OTiPc at (1, 0, 0; 1) is largest in phase II, where two OTiPc molecules form a slipped-stack conformation and two benzene units of one OTiPc lie on top of those of another OTiPc. This β value is much larger than that between OTiPc at (0, 0, 0; 0) and its neighbor at (0, 0, 0; 1), where the distance between two Ti atoms is closest (6.4 Å). This indicates that the β value is strongly dependent on the conformation between two OTiPc molecules. Indeed, the largest β_{HH} (1421 cm^{-1}) is twice as large as the largest β_{LL+1} (761 cm^{-1}), suggesting that an electron hole can move more easily than an excited electron. In the case of phase I, the resonance integral between OTiPc at (0, 0, 0; 0) and the neighboring OTiPc at (0, 0, 0; 2) is largest, but it is still smaller than the largest resonance integral in phase II. This is consistent with the experimental trend that the photocarrier generation efficiency is smaller in phase I than in phase II, demonstrating that the photoconductive properties correlate well with intermolecular resonance integrals.

Conclusions

Solid-state electronic absorption spectra of OTiPc have been theoretically calculated by considering three origins; exciton, CT, and molecular distortions. Our calculations have succeeded in reproducing several experimental trends (i.e., phase dependence, dependence on the incident light direction, and electroabsorption spectra), proving the reliability of our calculated results. In particular, we clarify for phase II that the large red shift and high CT character originate from large exciton interactions and large intermolecular resonance integrals, respectively, which result in the occurrence of near-IR-active photoconductivity. In addition, we reasonably demonstrate that the photoconductive properties correlate well with the intermolecular resonance integrals. The results shown in this report are important not only for investigating the electronic properties of molecular crystals but also for designing novel functional molecular crystals.[28−30]

Acknowledgment. This work was supported by a Grant-in-Aid for Scientific Research no. 14703007 from the Japan Society for the Promotion of Science, that for Scientific Research on Priority Area "Diagnosis and Treatment of Cancer" No. 15025212, from the Ministry of Education, Culture, Sports, Science and Technology, Japan, and that for the COE project Giant Molecules and Complex Systems, 2003, from the Ministry of Education, Culture, Sports, Science, and Technology, Japan.

References and Notes

(1) Nalwa, S.; Shirk, J. A. In *Phthalocyanines: Properties and Applications*; Leznoff, C. C., Lever, A. B. P., Eds.; VCH Publishers: New York, 1996; Vol. 4, Chapter 3.

(2) (a) Lever, A. B. P.; Hempstead, M. R.; Leznoff, C. C.; Liu, W.; Melnik, M.; Nevin, W.; Seymour, P. *Pure Appl. Chem.* **1986**, *18*, 1467. (b) Limson, J.; Nyokong, T. *Electroanalysis* **1997**, *9*, 255. (c) Hanabusa, K.; Shirai, H. In *Phthalocyanines: Properties and Applications*; Leznoff, C. C., Lever, A. B. P., Eds.; VCH Publishers: New York, 1993; Vol. 2, Chapter 5. (d) Kasuga, H. In *Phthalocyanines: Properties and Applications*; Leznoff, C. C., Lever, A. B. P., Eds.; VCH Publishers: New York, 1996; Vol. 4, Chapter 5. (e) Meunier, H.; Sorokin, A. *Acc. Chem. Res.* **1997**, *30*, 470.

(3) (a) Simon, J.; Bassoul, P. In *Phthalocyanines: Properties and Applications*; Leznoff, C. C., Lever, A. B. P., Eds.; VCH Publishers: New York, 1993; Vol. 2, Chapter 6. (b) Ng, D. K. P.; Yeung, Y.-O.; Chan, W. K.; Yu, S.-C. *Tetrahedron Lett.* **1997**, *38*, 6701.

(4) (a) Collins, G. C. S.; Schiffrin, D. J. *J. Electroanal. Chem.* **1982**, *139*, 335. (b) Nicholson, M. M. In *Phthalocyanines: Properties and Applications*; Leznoff, C. C., Lever, A. B. P., Eds.; VCH Publishers: New York, 1993; Vol. 3, Chapter 2. (c) Toshina, N.; Tominaga, T. *Bull. Chem. Soc. Jpn.* **1996**, *69*, 2111.

(5) (a) Morishige, K.; Tomoyasu, S.; Iwano, G. *Langmuir* **1997**, *13*, 5184. (b) Snow, A. W.; Barger, W. R. In *Phthalocyanines: Properties and Applications*; Leznoff, C. C., Lever, A. B. P., Eds.; VCH Publishers: New York, 1989; Vol. 1, Chapter 5.

(6) (a) Rosenthal, I.; Ben-Hur, E. In *Phthalocyanines: Properties and Applications*; Leznoff, C. C., Lever, A. B. P., Eds.; VCH Publishers: New York, 1989; Vol. 1, Chapter 6. (b) Daziano, J.-P.; Steenken, S.; Chabannon, C.; Mannoni, P.; Chanon, M.; Julliard, M. *Photochem. Photobiol.* **1996**, *64*, 712. (c) Anderson, C.; Hrabovsky, S.; McKinley, Y.; Tubesing, K.; Tang, H.-P.; Dunbar, R.; Makhtar, H.; Elmets, C. A. *Photochem. Photobiol.* **1997**, *65*, 895. (d) He, J.; Larkin, H. E.; Li, Y.-S.; Rihter, B. D.; Zaidi, S. I. A.; Rodgers, M. A. J.; Mukhtar, H.; Kenney, M. E.; Oleinick, N. L. *Photochem. Photobiol.* **1997**, *65*, 581.

(7) Simic-Glavaski, B. In *Phthalocyanines: Properties and Applications*; Leznoff, C. C., Lever, A. B. P., Eds.; VCH Publishers: New York, 1993; Vol. 3, Chapter 3.

(8) (a) Wohrle, D.; Kreienhoop, L.; Schlettwein, D. In *Phthalocyanines: Properties and Applications*; Leznoff, C. C., Lever, A. B. P., Eds.; VCH Publishers: New York, 1996; Vol. 4, Chapter 6. (b) Yonehara, H.; Pac, C. *Thin Solid Films* **1996**, *278*, 108.

(9) Rella, R.; Serra, A.; Siciliano, P.; Topore, A.; Valli, L.; Zocco, A. *Langmuir* **1997**, *13*, 6562.

(10) (a) Simon, J.; Andre, J. J. *Molecular Semiconductors*; Springer: Berlin, 1985. (b) Simon, J.; Toupance, T. In *Comprehensive Supramolecular Chemistry*; Reinhoudt, D. N., Ed.; Pergamon: London, 1996; Vol. 10, p 637. (c) McKeown, N. B. In *Phthalocyanine Materials: Synthesis, Structure and Function. Chemistry of Solid State Materials*; Cambridge University Press: New York, 1998; Vol. 6.

(11) Tanaka, M.; Koma, S. *Phthalocyanines—Basic Physical Properties and Application to Functional Materials*; Bunshin Publishers: Tokyo, 1991 (in Japanese).

(12) (a) Saito, T.; Sisk, W.; Kobayashi, T.; Suzuki, S.; Iwayanagi, T. *J. Phys. Chem.* **1993**, *97*, 8026. (b) Saito, T.; Iwakabe, Y.; Kobayashi, T.; Suzuki, S.; Iwayanagi, T. *J. Phys. Chem.* **1994**, *98*, 2726.

(13) Yamaguchi, S.; Sasaki, Y. *Chem. Phys. Lett.* **2000**, *323*, 35.

(14) Yonehara, H.; Etori, H.; Engel, M. K.; Tsushima, M.; Ikeda, N.; Ohno, T.; Pac, C. *Chem. Mater.* **2001**, *13*, 1015.

(15) Chau, L.-K.; England, C. D.; Chen, S.; Armstrong, N. R. *J. Phys. Chem.* **1993**, *97*, 2699.

(16) Sakakibara, Y.; Bera, R. N.; Mizutani, T.; Ishida, K.; Tokumoto, M.; Tani, T. *J. Phys. Chem. B* **2001**, *105*, 1547.

(17) (a) Oka, K.; Okada, O.; Nukada, K. *Jpn. J. Appl. Phys.* **1992**, *31*, 2181. (b) Okada, O.; Oka, K.; Iijima, M. *Jpn. J. Appl. Phys.* **1993**, *32*, 3556. (c) Okada, O.; Klein, M. L. *J. Chem. Soc., Faraday Trans.* **1996**, *92*, 2463. (d) Okada, O.; Klein, M. L. *Phys. Chem. Chem. Phys.* **2001**, *3*, 1530.

(18) Hillar, W.; Strähle, J.; Kovel, W.; Hanack, M. *Z. Kristallogr.* **1982**, *159*, 173.

(19) Mizuguchi, J.; Rihs, G.; Karfunkel, H. R. *J. Phys. Chem.* **1995**, *99*, 16217.

(20) Davydov, A. S. *Sov. Phys. −Usp.* **1964**, *530*, 145.

(21) (a) Parson, W. W.; Creighton, S.; Warshel, A. *J. Am. Chem. Soc.* **1989**, *111*, 4277. (b) Warshel, A.; Parson, W. W. *J. Am. Chem. Soc.* **1987**, *109*, 6143.

(22) (a) Ridley, J.; Zerner, M. *Theor. Chim. Acta* **1973**, *32*, 111. (b) Bacon, A. D.; Zerner, M. C. *Theor. Chim. Acta* **1979**, *53*, 21. (c) Zerner, M. C.; Loew, G. H.; Kirchner, R. F.; Mueller-Westerhoff, U. T. *J. Am. Chem. Soc.* **1980**, *102*, 589. (d) de Mello, P. C.; Hehenberger, M.; Larsson, S.; Zerner, M. *J. Am. Chem. Soc.* **1980**, *102*, 1278. (e) Anderson, W. P.; Edwards, W. D.; Zerner, M. C. *Inorg. Chem.* **1986**, *25*, 2728. (f) Anderson, W. P.; Cundari, T. R.; Drago, R. S.; Zerner, M. C. *Inorg. Chem.* **1990**, *29*, 1.

(23) *HyperChem* 5.1 Pro software package; Hypercube, Inc.: Gainesville, FL, **1997**.

(24) Kobayashi, N.; Konami, H. In *Phthalocyanines: Properties and Applications*; Wiley-VCH: Weinheim, Germany, 1996; Vol. 4, Chapter 9.

(25) (a) Reimers, J. R.; Hush, N. S. *J. Am. Chem. Soc.* **1995**, *117*, 1302. (b) Zeng, J.; Hush, N. S.; Reimers, J. R. *J. Phys. Chem.* **1995**, *99*, 10459.

(26) The $\sigma(\nu)$ function was evaluated as $(\nu - 7000)/15$ cm^{-1} from band-deconvolution analyses of phthalocyanine derivatives. Kobayashi, N.; Fukuda, T.; Lelièvre, D. *Inorg. Chem.* **2000**, *39*, 3632.

(27) Ogawa, K.; Yao, J.; Yonehara, H.; Pac, C. *J. Mater. Chem.* **1996**, *6*, 143.

(28) It is well-known that OTiPcs exhibit large third-order nonlinear optical susceptibility, χ^3.[29] To investigate this origin, the second hyperpolarizabilities, γ, were calculated for single OTiPc molecules in phases I and II, using the THG keyword of MOS-F 4.2D in the WinMOPAC 3.0 pro package.[30] The γ value (10^{-36} cm^6 erg^{-1}) calculated for phase II (-1517) is larger than that for phase I (-1250), which is consistent with the experimental results.

(29) Hosoda, M.; Wada, T.; Yamada, A.; Garito, A. F.; Sasabe, H. *Jpn. J. Appl. Phys.* **1991**, *30*, L1486.

(30) Matsuura, A. MOS-F 4.2D, Fujitsu Ltd: Tokyo, 2000.